Ozone Oxidation of Surface-Adsorbed Polycyclic Aromatic Hydrocarbons: Role of PAH−Surface Interaction

Sophie N. Chu, Sophia Sands, Michelle R. Tomasik,[†] Paul S. Lee, and V. Faye McNeill*

Department of Chemical Engineering, Columbia University, New York, New York 10027, United States

Received February 19, 2010; E-mail: vfm2103@columbia.edu

Abstract: The heterogeneous chemistry of surface-adsorbed polycyclic aromatic hydrocarbons (PAHs) plays key roles in nanoscience, environmental science, and public health. Experimental evidence shows that the substrate can influence the heterogeneous oxidation of surface-bound PAHs, however, a mechanistic understanding of the role of the surface is still lacking. We examine the effects of the PAH−substrate interaction on the oxidation of surface-adsorbed anthracene, pyrene, and benzo[*a*]pyrene by ozone (O_3) using density functional theory. We find that some O_3 oxidation mechanisms for these planar PAH molecules lead to nonplanar intermediates or products, the formation of which may necessitate partial desorption or "lift-off" from a solid substrate. The energy penalty for partial desorption of each PAH from the surface is estimated for four different substrate types on the basis of literature data and accounted for in the thermodynamic analysis of the reaction pathways. We find that the attractive PAH−substrate interaction may render oxidation pathways involving nonplanar intermediates or products thermodynamically unfavorable. The influence of the PAH−substrate interaction could contribute in part to the variations in PAH oxidation kinetics and product distributions that have been observed experimentally. Our choice of test molecules enabled us to identify trends in reactivity and product formation for four types of potentially reactive site (zigzag, armchair, bridge, and internal), allowing us to infer products and mechanisms of O_3 oxidation for PAHs of larger sizes. Implications for atmospheric chemistry and the stability of graphene in the presence of O_3 are discussed.

Introduction

Molecules in the polycyclic aromatic hydrocarbon (PAH) family range in scale from a few fused benzene rings to micrometer-scale graphene sheets. Small (six or fewer rings) PAHs are byproducts of combustion that are prevalent in the environment.[1] PAHs consisting of three or more fused aromatic rings have relatively low vapor pressures and will therefore partition to atmospheric aerosol particles and other environmental surfaces, where they may react with O_3 and other atmospheric oxidants. Small PAHs and their oxidation products have well-documented adverse effects on human health.[2] A mechanistic understanding of the O_3 oxidation of PAHs is necessary for evaluating their environmental fates and human exposure to them.[1,3−12]

The heterogeneous oxidation kinetics of small PAHs have been observed to vary depending on the identity of the substrate; however, the role of the surface is still unclear.[6−12] Experimental studies of the oxidation of surface-adsorbed anthracene, benzo[*a*]pyrene (B[*a*]P), and pyrene by gas-phase O_3 have shown that these systems generally follow Langmuir−Hinshelwood-type kinetics. That is, when O_3 concentrations in the gas phase are low, the rate of PAH loss increases with increasing O_3 concentration and then eventually saturates according to[13]

$$k^I = k^I_{max} \frac{K_{O3}[O_3]}{1 + K_{O3}[O_3]} \tag{1}$$

where k^I is the first-order rate constant, k^I_{max} is the maximum first-order rate constant that is observed when the surface is

† Current affiliation: Department of Physics, Massachusetts Institute of Technology, Cambridge, MA 02139.

(1) Finlayson-Pitts, B. J.; Pitts, J. N. *Chemistry of the Upper and Lower Atmosphere: Theory, Experiments, And Applications*, 1st ed.; Academic Press: San Diego, 2000.

(2) World Health Organization. *Environmental Health Criteria 202: Selected Non-heterocyclic Aromatic Hydrocarbons*; WHO: Geneva, 1998.

(3) Finlayson-Pitts, B. J.; Pitts, J. N. *Science* 1997, 276, 1045–1052.

(4) Pitts, J. N.; Lokensgard, D. M.; Ripley, P. S.; Vancauwenberghe, K. A.; Vanvaeck, L.; Shaffer, S. D.; Thill, A. J.; Belser, W. L. *Science* 1980, 210, 1347–1349.

(5) Fox, M. A.; Olive, S. *Science* 1979, 205, 582–583.

(6) Poschl, U.; Letzel, T.; Schauer, C.; Niessner, R. *J. Phys. Chem. A* 2001, 105, 4029–4041.

(7) Kwamena, N. O. A.; Thornton, J. A.; Abbatt, J. P. D. *J. Phys. Chem. A* 2004, 108, 11626–11634.

(8) Kwamena, N. O. A.; Staikova, M. G.; Donaldson, D. J.; George, I. J.; Abbatt, J. P. D. *J. Phys. Chem. A* 2007, 111, 11050–11058.

(9) Gao, S.; Zhang, Y.; Meng, J.; Shu, J. *Atmos. Environ.* 2009, 43, 3319–3325.

(10) Kahan, T. F.; Kwamena, N. O. A.; Donaldson, D. J. *Atmos. Environ.* 2006, 40, 3448–3459.

(11) Mmereki, B. T.; Donaldson, D. J.; Gilman, J. B.; Eliason, T. L.; Vaida, V. *Atmos. Environ.* 2004, 38, 6091–6103.

(12) Kwamena, N. O. A.; Earp, M. E.; Young, C. J.; Abbatt, J. P. D. *J. Phys. Chem. A* 2006, 110, 3638–3646.

(13) Steinfeld, J. I.; Francisco, J. S.; Hase, W. L. *Chemical Kinetics and Dynamics*, 2nd ed.; Prentice Hall: Upper Saddle River, NJ, 1999.

saturated with ozone, K_{O3} is the adsorption equilibrium constant for ozone, and [O_3] is the gas-phase ozone concentration. Despite the similar functional dependence on [O_3], the inferred rate parameters K_{O3} and k_{max}^I have been observed to vary widely from study to study, depending on the substrate on which the PAH is adsorbed and the experimental method.[6−12]

Kwamena et al. proposed that the polarity of the substrate may control O_3 adsorption to the surface prior to reaction (i.e., K_{O3}), thus influencing the observed PAH loss kinetics.[8] Another way in which the substrate may influence PAH oxidation is via the PAH−substrate interaction. In their lowest-energy configurations, PAHs such as anthracene, benz[a]anthracene, B[a]P, and pyrene are planar in geometry. PAH adsorption onto graphitic surfaces including soot may be enhanced by $\pi-\pi$ interactions.[14] Oxidation mechanisms that necessitate partial detachment of the PAH molecule from the substrate may incur an energy penalty, thus affecting the thermodynamics of the reaction pathway.

Graphene, an extended PAH that may reach microscopic molecular dimensions, has unique and potentially useful electronic properties.[15−20] Chemical processing by gas-phase species could be an effective approach for controlled functionalization of graphene for applications in nanoscale devices[21−33] and may also provide new routes for fabrication of graphene sheets or nanoribbons.[23,29] Furthermore, as we move toward widespread use of graphene in commercial applications, its stability in the presence of atmospheric oxidants such as ozone and its environmental fate should be evaluated.[34−38] Relatively few

studies exist on the heterogeneous chemistry of surface-deposited graphene, but experimental evidence suggests that interactions with the substrate may play an important role: Liu et al. observed that O_2 oxidation reactions requiring "lift-off" were inhibited for graphene when adsorbed on graphite surfaces.[22]

Here we show via a suite of density functional theory calculations that steric effects on the PAH−substrate interaction may influence the mechanisms and products of PAH oxidation by O_3 on surfaces. We chose anthracene, pyrene, and B[a]P as model PAH compounds for this study because of their environmental importance and because abundant experimental data exist in the literature regarding the heterogeneous oxidation of these species and their surface interactions. Furthermore, B[a]P contains the full range of nondefect oxidation site types found in PAHs (edge, zigzag, armchair, internal), and therefore, a mechanistic understanding of its oxidation chemistry can provide insight into that of larger PAHs such as graphene. We find that, in some cases, the carbon skeleton of the oxidation products or reaction intermediates deviates significantly from the planar geometry of the PAH parent molecule, necessitating partial desorption or lift-off from a solid substrate. This departure from planar geometry may be inhibited by attractive interactions between the PAH molecule and the underlying substrate. The energy penalty for partial desorption from the surface for different particle types was estimated on the basis of literature data and incorporated into a thermodynamic analysis of the oxidation reaction pathways. Our results suggest that PAH−surface interactions influence their reactivity toward O_3 and the oxidation products formed.

Method

We performed a thermodynamic analysis of stable products and intermediates along the ozone oxidation pathways for anthracene, pyrene, and B[a]P, taking into account the PAH−surface interaction as described in the following sections. Our goal for this study was to screen these pathways for thermodynamic favorability; reactions we find to be thermodynamically favorable here could be kinetically limited. Our geometry-based analysis of the stable species nearest in free energy to the transition state for a given reaction pathway should also apply to that transition state.[39]

Ab Initio Calculations. Geometries were optimized and vibrational frequency calculations were performed via Jaguar 6.0 (Schrödinger) using density functional theory (DFT) with the B3LYP functional and the 6-31G** basis set. Unconstrained geometry optimizations were performed. The ab initio calculations are for gas-phase species and neglect any interaction of O_3 or the PAH with the underlying substrate; PAH−surface interaction was accounted for separately, as discussed in the following section. The free energy of each species was taken as the total Gibbs free energy, G_{tot}, at 298.15 K, which includes the self-consistent field (SCF) energy and the zero-point energy. The free energy of reaction was calculated on the basis of the total Gibbs free energy of the reactants and products in the usual manner:

$$\Delta G_{rxn} = \sum_i \nu_i G_{tot,i} \qquad (2)$$

where ν_i is the stoichiometric coefficient (negative for reactants, positive for products). No further corrections were applied.

(14) Kubicki, J. D. *Environ. Sci. Technol.* **2006**, *40*, 2298–2303.
(15) Novoselov, K. S.; Geim, A. K.; Morozov, S. V.; Jiang, D.; Zhang, Y.; Dubonos, S. V.; Grigorieva, I. V.; Firsov, A. A. *Science* **2004**, *306*, 666–669.
(16) Geim, A. K.; Novoselov, K. S. *Nat. Mater.* **2007**, *6*, 183–191.
(17) Zhang, Y. B.; Tan, Y. W.; Stormer, H. L.; Kim, P. *Nature* **2005**, *438*, 201–204.
(18) Bolotin, K. I.; Sikes, K. J.; Jiang, Z.; Klima, M.; Fudenberg, G.; Hone, J.; Kim, P.; Stormer, H. L. *Solid State Commun.* **2008**, *146*, 351–355.
(19) Eda, G.; Fanchini, G.; Chhowalla, M. *Nat. Nanotechnol.* **2008**, *3*, 270–274.
(20) Ratinac, K. R.; Yang, W.; Ringer, S. P.; Braet, F. *Environ. Sci. Technol.* **2010**, *44*, 1167–1176.
(21) Ruoff, R. S. *Nat. Nanotechnol.* **2008**, *3*, 10–11.
(22) Liu, L.; Ryu, S.; Tomasik, M. R.; Stolyarova, E.; Jung, N.; Hybertsen, M. S.; Steigerwald, M. L.; Brus, L. E.; Flynn, G. W. *Nano Lett.* **2008**, *8*, 1965–1970.
(23) Li, Z. Y.; Zhang, W. H.; Luo, Y.; Yang, J. L.; Hou, J. G. *J. Am. Chem. Soc.* **2009**, *131*, 6320–6321.
(24) Huang, B.; Li, Z. Y.; Liu, Z. R.; Zhou, G.; Hao, S. G.; Wu, J.; Gu, B. L.; Duan, W. H. *J. Phys. Chem. C* **2008**, *112*, 13442–13446.
(25) Ryu, S.; Han, M. Y.; Maultzsch, J.; Heinz, T. F.; Kim, P.; Steigerwald, M. L.; Brus, L. E. *Nano Lett.* **2008**, *8*, 4597–4602.
(26) Liu, H. T.; Ryu, S. M.; Chen, Z. Y.; Steigerwald, M. L.; Nuckolls, C.; Brus, L. E. *J. Am. Chem. Soc.* **2009**, *131*, 17099–17101.
(27) Bekyarova, E.; Itkis, M. E.; Ramesh, P.; Berger, C.; Sprinkle, M.; de Heer, W. A.; Haddon, R. C. *J. Am. Chem. Soc.* **2009**, *131*, 1336–1337.
(28) Wang, X. R.; Tabakman, S. M.; Dai, H. J. *J. Am. Chem. Soc.* **2008**, *130*, 8152–8153.
(29) Xiang, H. J.; Kan, E. J.; Wei, S. H.; Whangbo, M. H.; Yang, J. L. *Nano Lett.* **2009**, *9*, 4025–4030.
(30) Ouyang, F. P.; Huang, B.; Li, Z. Y.; Xiao, J.; Wang, H. Y.; Xu, H. *J. Phys. Chem. C* **2008**, *112*, 12003–12007.
(31) Cervantes-Sodi, F.; Csanyi, G.; Piscanec, S.; Ferrari, A. C. *Phys. Rev. B* **2008**, *77*.
(32) Elias, D. C.; Nair, R. R.; Mohiuddin, T. M. G.; Morozov, S. V.; Blake, P.; Halsall, M. P.; Ferrari, A. C.; Boukhvalov, D. W.; Katsnelson, M. I.; Geim, A. K.; Novoselov, K. S. *Science* **2009**, *323*, 610–613.
(33) Choi, J.; Lee, H.; Kim, K.-J.; Kim, B.; Kim, S. *J. Phys. Chem. Lett.* **2010**, *1*, 505–509.
(34) Behra, R.; Krug, H. *Nat. Nanotechnol.* **2008**, *3*, 253–254.
(35) Biswas, P.; Wu, C. Y. *J. Air Waste Manage. Assoc.* **2005**, *55*, 708–746.
(36) Scheringer, M. *Nature Nanotechnol.* **2008**, *3*, 322–323.
(37) Wiesner, M. R.; Lowry, G. V.; Alvarez, P.; Dionysiou, D.; Biswas, P. *Environ. Sci. Technol.* **2006**, *40*, 4336–4345.
(38) Mueller, N. C.; Nowack, B. *Environ. Sci. Technol.* **2008**, *42*, 4447–4453.
(39) Hammond, G. S. *J. Am. Chem. Soc.* **1955**, *77*, 334–338.

The B3LYP/6-31G** level of theory is standard and has been used in other studies of graphene and PAHs.[40,41] This method was found to predict the geometry of anthracene well ($\chi^2 = 6.34 \times 10^{-4}$ Å) as compared to experimental observations.[42] The calculated total enthalpy of reaction for anthraquinone formation at 298.15 K differed from that derived using standard heats of formation from the NIST Webbook[43] by 2.6 kcal mol^{-1}. Full details of the comparisons with experimental data, as well as the optimized geometries and energies for all species, can be found in the Supporting Information.

PAH−Surface Interaction Energy. The products and/or reaction intermediates of some, but not all, of the oxidation reactions studied here exhibit nonplanar geometry that would necessitate partial desorption or lift-off from a solid substrate. For these systems, whether or not oxidation will be thermodynamically favorable depends on the change in free energy of the oxidation reaction and the free energy penalty for partial desorption of the PAH molecule from the surface. We estimate that the partial desorption energy is proportional to the energy of complete desorption from the surface, ΔG_{des}, scaled by the degree of desorption, ζ, which we define as the fraction of carbon atoms that leave the plane. The reaction will be thermodynamically favorable if

$$\Delta G_{rxn} + \zeta \Delta G_{des} \leq 0 \tag{3}$$

Note that in the formation of a planar product molecule from any nonplanar intermediate, the energy penalty of partial desorption may be recovered. The degree of desorption for a given structure was quantified in this study as follows: the root mean squared (rms) deviation from planarity, δ, of each carbon atom was analyzed using ChemBio3D Ultra 11.0 software (Cambridgesoft Corp.). A carbon atom was considered to have desorbed from the surface if $\delta > 0.10$ Å.

We assume here that the substrate is planar on the length scale of the PAH molecule. Atmospheric aerosol particles may have a variety of morphologies including spheres, crystals with planar faces, or irregular shapes.[1] However, the relatively large size of most particles compared to a small PAH molecule suggests that it is reasonable to assume that the reaction site is locally planar. This analysis does not take into account the effects of nanoscale surface roughness or inhomogeneities such as step edges. We also note that, besides surface adsorption, PAH molecules may also partition to atmospheric aerosols via absorption into an aerosol organic phase, a scenario that is not considered here.[44]

ΔG_{des} values for anthracene and pyrene desorbing from different particle types were derived from literature data as described in the following paragraphs. The ΔG_{des} data are summarized in Table 1. Following the Langmuir model convention and assuming barrierless adsorption, we can write the Arrhenius expression for desorption as[45]

$$k_{des} = A \exp\left(-\frac{\Delta G_{des}}{RT}\right) \tag{4}$$

where k_{des} is the desorption rate constant, R is the gas constant, T is temperature, and A is the Arrhenius prefactor. Thus, it follows that

Table 1. Desorption Energies for Anthracene and Pyrene from Different Particle Types, Calculated As Described in the Text

PAH	particle type	ΔG_{des} (kcal mol^{-1})	ref
anthracene	kerosene soot	21.0 ± 0.8	47
	fly ash	24.3	48
	NaCl	18.0 ± 1.0	a
phenanthrene/anthracene	urban aerosol	18.9	49, 51
pyrene	kerosene soot	22.7 ± 0.4	46
	fly ash	26.6	48
	NaCl	19.6 ± 0.9	a
	urban aerosol	20.4	49, 51
benzo[a]pyrene	kerosene soot	29.1 ± 1.1	47
	fly ash	31.2 ± 0.8	b
	NaCl	22.8 ± 0.5	b
benzo[a]pyrene/benzo[e]pyrene	urban aerosol	22.3	49, 51

^{a} Estimated on the basis of data for perylene from refs 52 and 53. ^{b} Extrapolated from data for anthracene and pyrene. See the text for details.

$$\ln K = a_1 + \frac{\Delta G_{des}}{RT} \tag{5}$$

where K is the adsorption equilibrium constant, k_{ads}/k_{des}. Guilloteau et al. measured the desorption of anthracene, pyrene, and B[a]P from kerosene soot surfaces.[46,47] On the basis of their data and eq 5, we find that $\Delta G_{des} = 21.0 \pm 0.8$, 22.7 ± 0.4, and 29.1 ± 1.1 kcal mol^{-1} for anthracene, pyrene, and B[a]P, respectively (the uncertainties reflect the reported uncertainties in the experimental data).[46,47] Applying eq 5 to the data of Lee et al. for anthracene and pyrene desorption from municipal incinerator fly ash, we calculated $\Delta G_{des} = 24.3$ kcal mol^{-1} for anthracene and 26.6 kcal mol^{-1} for pyrene.[48]

ΔG_{des} values may also be extracted from temperature-dependent gas-particle partitioning data from atmospheric aerosol studies. Data analysis in these studies generally follows the convention of Pankow's gas-particle partitioning theory for the adsorption of semivolatile compounds to solid particles[49,50]

$$\log_{10} K = \frac{m_p}{T} + b_p \tag{6}$$

where m_p and b_p are fit parameters that can be related to the enthalpy of desorption, aerosol surface area, and properties of the adsorbate. Converting the base 10 logarithm to natural logarithm and comparing eqs 5 and 6 we find that

$$\Delta G_{des} = 2.303 R m_p \tag{7}$$

On the basis of Pankow's reanalysis of the data of Yamasaki et al. for gas-particle partitioning of PAHs to ambient urban aerosol of mixed composition, we calculate ΔG_{des} values of 18.9 kcal mol^{-1} for anthracene, 20.4 kcal mol^{-1} for pyrene, and 22.3 kcal mol^{-1} for B[a]P.[51,49]

To our knowledge, no studies exist in the literature of anthracene and pyrene surface adsorption onto NaCl or other inorganic salt particles. Steiner and Burtscher found that the enthalpy of desorption for perylene, a five-ring PAH, from 60 nm NaCl particles was

(40) Lu, X.; Zhang, L. L.; Xu, X.; Wang, N. Q.; Zhang, Q. N. *J. Phys. Chem. B* **2002**, *106*, 2136–2139.

(41) Cohen, Y. S.; Xiao, S. X.; Steigerwald, M. L.; Nuckolls, C.; Kagan, C. R. *Nano Lett.* **2006**, *6*, 2838–2841.

(42) Ketkar, S. N.; Kelley, M.; Fink, M.; Ivey, R. C. *J. Mol. Struct.* **1981**, *77*, 127–138.

(43) Afeefy, H. Y.; Liebman, J. F.; Stein, S. E. *NIST Chemistry Webbook, NIST Standard Reference Database Number 69*; National Institute of Standards and Technology: Gaithersburg, MD, 2010.

(44) Seinfeld, J. H.; Pandis, S. N. *Atmospheric Chemistry and Physics: From Air Pollution to Climate Change*, 2nd ed.; Wiley: New York, 2006.

(45) Adamson, A. W.; Gast, A. P. *Physical Chemistry of Surfaces*, 6th ed.; Wiley: New York, 1997.

(46) Guilloteau, A.; Nguyen, M. L.; Bedjanian, Y.; Le Bras, G. *J. Phys. Chem. A* **2008**, *112*, 10552–10559.

(47) Guilloteau, A.; Bedjanian, Y.; Nguyen, M. L.; Tomas, A. *J. Phys. Chem. A* **2010**, *114*, 942–948.

(48) Lee, W. M. G.; Chen, J. C. *Environ. Int.* **1995**, *21*, 827–831.

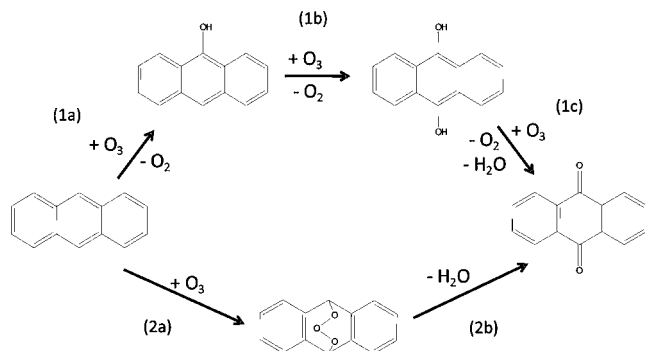(49) Pankow, J. F. *Atmos. Environ.* **1991**, *25*, 2229–2239.

(50) Pankow, J. F. *Atmos. Environ.* **1987**, *21*, 2275–2283.

(51) Yamasaki, H.; Kuwata, K.; Miyamoto, H. *Environ. Sci. Technol.* **1982**, *16*, 189–194.

(52) Steiner, D.; Burtscher, H. K. *Environ. Sci. Technol.* **1994**, *28*, 1254–1259.

(53) Hueglin, C.; Paul, J.; Scherrer, L.; Siegmann, K. *J. Phys. Chem. B* **1997**, *101*, 9335–9341.

Figure 1. Production of anthraquinone, based on the reaction mechanism suggested by Bailey.[58]

approximately 4 kcal/mol lower than that for desorption from carbon (soot) particles or combustion particles of similar size.[52] Hueglin et al. found a smaller difference in the desorption energies of perylene from NaCl and carbon particles; their results for carbon particles could be described by using a model of two types of equally populated surface sites, one type having the same ΔG_{des} as NaCl and the other having 4% higher ΔG_{des}.[53] On the basis of these two studies, we expect that the difference in desorption energies between these two substrates for anthracene and pyrene is ≤4 kcal/mol. That is, referring to the data from Guilloteau et al. for the desorption of anthracene and pyrene from soot, for an NaCl substrate, we calculate $\Delta G_{des} \geq 17.0$ kcal mol^{-1} for anthracene and $\Delta G_{des} \geq 18.7$ kcal mol^{-1} for pyrene.[46,47] It is also expected that these PAHs will exhibit weaker binding to NaCl than to urban aerosol such as that studied by Yamasaki et al., which is likely to consist of a mixture of many particle types including inorganic salts and combustion aerosol.[51] We can use the desorption energies for anthracene and pyrene from urban aerosol that we derived from the data of Yamasaki et al. as upper bounds for the NaCl desorption energies. Therefore, on the basis of the available data, we estimate ΔG_{des} for desorption from NaCl to be 18.0 ± 1.0 kcal mol^{-1} for anthracene and 19.6 ± 0.9 kcal mol^{-1} for pyrene.

Experimental data are also lacking for B[*a*]P desorption from NaCl or fly ash substrates. We observed that ΔG_{des} follows a linear dependence on the number of carbon atoms in the PAH molecule for the other two particle types studied here. This is consistent with experimental studies of the adsorption of alkyl alcohols and simple alkanes on graphite or metals, which show a linear dependence of the desorption energy on carbon number for species with 20 or fewer carbon atoms.[54−57] Therefore, using linear extrapolations from the anthracene and pyrene data, we estimate $\Delta G_{des} = 22.8 \pm 0.5$ kcal mol^{-1} for B[*a*]P on NaCl and $\Delta G_{des} = 31.2 \pm 0.8$ kcal mol^{-1} for B[*a*]P on fly ash.

Results and Discussion

Mechanism of Anthraquinone Formation. Mmereki et al. presented a two-pathway mechanism, originally proposed by Bailey, for anthracene (AN) oxidation to form 9,10-anthraquinone (AQ), shown in Figure 1.[11,58] Pathway 1 involves the formation of hydroxyl intermediates and three successive

(54) Zhang, R. M.; Gellman, A. J. *J. Phys. Chem.* **1991**, *95*, 7433–7437.
(55) Wetterer, S. M.; Lavrich, D. J.; Cummings, T.; Bernasek, S. L.; Scoles, G. *J. Phys. Chem. B* **1998**, *102*, 9266–9275.
(56) Teplyakov, A. V.; Gurevich, A. B.; Yang, M. X.; Bent, B. E.; Chen, J. G. G. *Surf. Sci.* **1998**, *396*, 340–348.
(57) Paserba, K. R.; Gellman, A. J. *Phys. Rev. Lett.* **2001**, *86*, 4338–4341.
(58) Bailey, P. *Ozonation in Organic Chemistry*; Academic Press: New York, 1982.
(59) Ardura, D.; Donaldson, D. J. Personal communication, 2009.
(60) Perraudin, E.; Budzinski, H.; Villenave, E. *Atmos. Environ.* **2007**, *41*, 6005–6017.

Table 2. Energetics of Anthracene Oxidation Pathways Shown in Figures 1 and 2

reaction	ΔG_{rxn} (kcal mol^{-1}) B3LYP/6-31G**	degree of desorption, ζ	$\Delta G_{rxn} + \zeta\Delta G_{des}$ (kcal mol^{-1})			
			fly ash	soot	NaCl	urban aerosol
1a	−41.5	0	−41.5			
1a′	−1.09	3/14	+4.11	+3.40	+2.76	+2.95
1b	−40.5	0	−40.5			
1c	−60.3	0	−60.3			
2a	−21.3	10/14	−3.94	−6.3	−8.44	−7.8
2b	−138.6	−10/14	−156.0	−153.6	−151.5	−152.1

additions of O_3 to anthracene, to result in the following overall stoichiometry for the pathway:

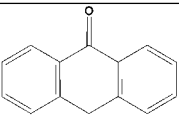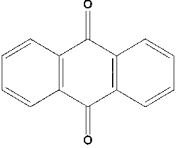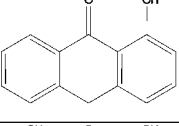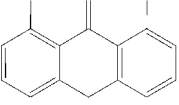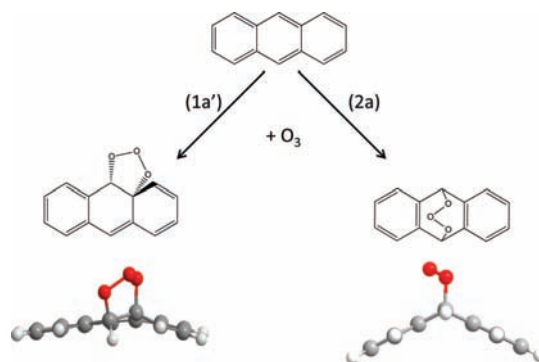$$AN + 3O_3 \rightarrow AQ + 3O_3 + H_2O \qquad (R1)$$

In the second pathway, ozone bonds to C9 and C10 of the anthracene to form a bridgelike intermediate which then decomposes to form AQ and H_2O. The stoichiometry is

$$AN + O_3 \rightarrow AQ + H_2O \qquad (R2)$$

We performed energy calculations for both pathways. The results of the calculations are summarized in Table 2. Both pathways are thermodynamically favorable, with a net ΔG_{rxn} of −143 and −160 kcal mol^{-1} for pathways 1 and 2, respectively (they are not the same due to the different stoichiometry of the two pathways). However, the optimized geometry for the bridge intermediate in pathway 2 is nonplanar, with all but four carbon atoms lifting from the surface (see Figure 2). ΔG_{rxn} for the formation of this intermediate is calculated to be −21.3 kcal mol^{-1}. When the energy penalty for partial desorption is taken into account, the total energy change for the process is smaller in magnitude but still negative for each particle type studied, with $\Delta G_{rxn} + \zeta\Delta G_{des} = -6.3$ kcal mol^{-1} for kerosene soot particles. The intermediates in pathway 1 of the Bailey mechanism as well as the 9,10-anthraquinone product are planar.

The Bailey mechanism was recently updated by Ardura and Donaldson on the basis of insight provided by ab initio calculations.[59] They found that pathways 1 and 2 of the Bailey mechanism both involve the formation of hydroxyl intermediates and three successive additions of O_3 to anthracene, such that each pathway has the overall stoichiometry of eq R1R1.

A schematic of the first O_3 addition steps for both pathways is shown in Figure 2. In pathway 1, each O_3 attacks a double bond in the center ring of anthracene. Pathway 2 proceeds via the formation of a bridgelike intermediate as in the Bailey mechanism.

Figure 2. Initiation of anthracene oxidation by O_3, based on the reaction mechanism suggested by Ardura and Donaldson.[59]

Table 3. Products of the Ozone Oxidation of Surface-Bound Anthracene Proposed by Gloaguen et al.[61] Which Were Predicted To Have Planar Geometry[a]

Molecule	ΔG_{rxn} (kcal mol^{-1}) B3LYP/6-31G**
a)	-48.7
b)	-143 (pathway (1)) -160 (pathway (2))
c)	-81.6
d)	-137

[a] ΔG_{rxn} values calculated in this study are shown.

On the basis of our calculations, the initial O_3 addition reaction for pathway 1 as proposed by Ardura and Donaldson is thermodynamically favorable, with $\Delta G_{rxn} = -1.09$ kcal mol^{-1}. The optimized geometry is nonplanar, although the distortion is not as significant as for the pathway 2 intermediate (see Figure 2). However, because of the relatively small magnitude of ΔG_{rxn}, we find that $\Delta G_{rxn} + \zeta\Delta G_{des}$ is positive (i.e., not thermodynamically favorable) for each particle type studied. This suggests that pathway 1 for 9,10-anthraquinone formation will be inhibited for anthracene adsorbed to a soot, NaCl, fly ash, or urban aerosol surface.

Inhibition of one anthracene−ozone oxidation pathway could result in a reduction in the observed rates of anthraquinone formation and anthracene loss. Therefore, the PAH−substrate interaction could contribute in part to the wide variation in anthracene loss kinetics that has been observed experimentally.[8] In the context of the Langmuir−Hinshelwood mechanism, the PAH−substrate interaction will influence k_{max}^I. Perraudin et al. found that the second-order rate constant ($kII \cong k_{max}^I K_{O3}$) was significantly higher for the ozone oxidation of anthracene adsorbed on silica particles as compared to graphite particles.[60] Silica, a more polar substrate, is predicted to have a lower value
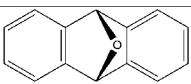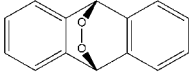
of K_{O3} than graphite, thus suggesting a lower k^{II} value for silica.[8] However, the anthracene−silica interaction is predicted to be weaker than the anthracene−graphite interaction, which is enhanced by $\pi-\pi$ stacking. This, in the context of our results, suggests a higher value of k_{max}^I for silica than graphite, consistent with the observations of Perraudin et al.

Other Anthracene Oxidation Products. We have applied the desorption penalty approach to investigate the products proposed by Gloaguen et al. for the ozone oxidation of anthracene adsorbed on dry NaCl particles.[61] The results are summarized in Tables 3 and 4. The species listed in Table 3 are planar, and their formation is net thermodynamically favorable. While we have not done detailed studies on the formation mechanisms for these species from the reaction of anthracene with O_3, we anticipate that the mechanisms are analogous to the mechanisms proposed in the literature for 9,10-anthraquinone formation. Therefore, nonplanar intermediates may be involved, and the PAH−surface interaction may influence the formation of these species. The epoxide and endoperoxide species in Table 4 are nonplanar, and $\Delta G_{rxn} + \zeta\Delta G_{des}$ values for their formation are positive for each particle type analyzed here, including NaCl. Therefore, our calculations do not support the formation of the species listed in Table 4 in the experimental system of Gloaguen et al.[61] It is more probable that the isomers of these species, molecules a and c in Table 3, are responsible for the observed peaks in the mass spectra.

Ozone Oxidation of Surface-Adsorbed Pyrene. O_3 oxidation has been reported to result in ring-opening via a Criegee mechanism for benz[a]anthracene and pyrene.[9,62−64] To our knowledge, open-ring products have not been observed experimentally to result from the reaction of anthracene with O_3. The formation of a Criegee intermediate (shown in Figure 3) results in significant lift-off from the substrate surface. Therefore, we hypothesize that this pathway may be inhibited when the PAH−substrate interaction is sufficiently strong.

The results of our energy calculations for pyrene ozonolysis via the Criegee mechanism are summarized in Table 5. ΔG_{rxn} for the second step in the Criegee mechanism (the formation of the Criegee intermediate from the primary ozonide) is positive, even though the resulting molecule is a lower-energy state than the reactants (pyrene and O_3). A free energy diagram for this reaction pathway is shown in Figure 4. Significant distortion of the molecule occurs when the Criegee intermediate is formed, such that most of the carbon atoms must lift off from the surface. The energy penalty for partial desorption from any particle type is sufficient to increase the free energy of the Criegee intermediate to higher than that of the reactants (pyrene and O_3), that is, ring-opening may be inhibited for surface-

Table 4. Products of the Ozone Oxidation of Surface-Bound Anthracene Proposed by Gloaguen et al.[61] Which Were Predicted To Have Nonplanar Geometry[a]

	Molecule	ΔG_{rxn} (kcal mol^{-1}) B3LYP/6-31G**	Degree of desorption, ζ	$\Delta G_{rxn}+\zeta\Delta G_{des}$ (kcal mol^{-1})			
				Fly ash	Soot	NaCl	Urban aerosol
e)		-7.82	10/14	+9.54	+7.18	+5.04	+5.68
f)		-11.4	10/14	+5.96	+3.6	+1.46	+2.1

[a] ΔG_{rxn} values calculated in this study are shown, alone and accounting for the energy penalty of partial desorption. See the text for details.
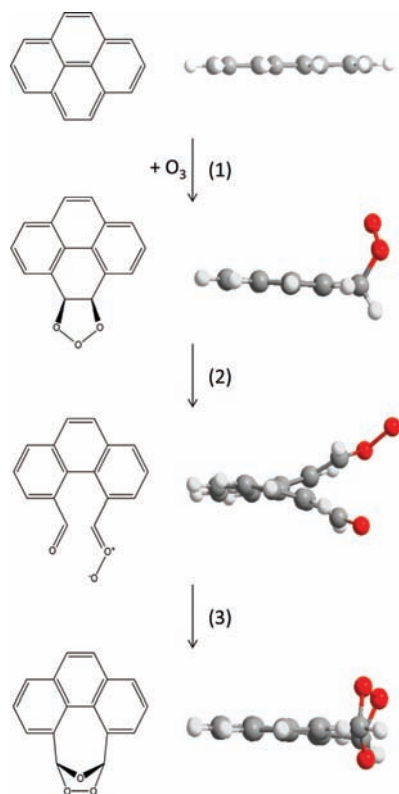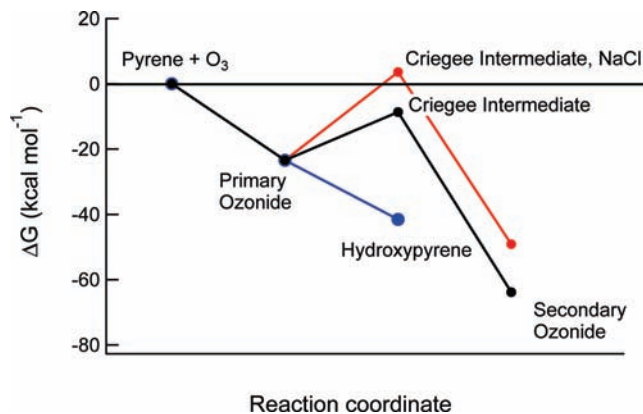
Figure 3. Pyrene ozonolysis via the Criegee mechanism. Each species is shown in profile to demonstrate the distortions from the planar geometry of pyrene. Note that other products besides the secondary ozonide may form from the Criegee intermediate.

Figure 4. Free energy diagram for hydroxypyrene (blue line) and secondary ozonide formation (red line, PAH adsorbed on NaCl surface; black line, no PAH−surface interaction) from pyrene + O_3.

Table 5. Energetics of Pyrene Oxidation Reaction Steps Shown in Figure 3

reaction	ΔG_{rxn} (kcal mol^{-1}) B3LYP/6-31G**	degree of desorption, ζ	$\Delta G_{rxn} + \zeta\Delta G_{des}$ (kcal mol^{-1})			
			fly ash	soot	NaCl	urban aerosol
1	−23.4	0			−23.4	
2	+14.8	10/16	+31.4	+28.9	+27.0	+27.5
3	−55.2	0			−55.2	

adsorbed pyrene. Gao et al. observed the formation of hydroxy-pyrene in addition to ring-opening products after exposing pyrene-coated NaCl particles to ozone.[9] In Figure 5, we propose a formation pathway for hydroxypyrene from the primary ozonide. This pathway is represented in Figure 4 as a blue line. No significant distortion of the pyrene backbone is necessary in this mechanism, which is consistent with the observation of hydroxypyrene formation from pyrene adsorbed on NaCl particles. Hydroxypyrene is a higher-energy product than the secondary ozonide and other possible products formed by the Criegee mechanism,[65] indicating that in the absence of the PAH−surface interaction its formation would be less favorable. Hydroxypyrene was not reported as a product for the ozone oxidation of pyrene dissolved in acetonitrile/water solution.[64]

(61) Gloaguen, E.; Mysak, E. R.; Leone, S. R.; Ahmed, M.; Wilson, K. R. *Int. J. Mass Spec.* **2006**, *258*, 74–85.
(62) Moriconi, E. J.; Oconnor, W. F.; Wallenberger, F. T. *J. Am. Chem. Soc.* **1959**, *81*, 6466–6472.
(63) Yao, J. J.; Huang, Z. H.; Masten, S. J. *Water Res.* **1998**, *32*, 3235–3244.
(64) Yao, J. J.; Huang, Z. H.; Masten, S. J. *Water Res.* **1998**, *32*, 3001–3012.
(65) Epstein, S. A.; Donahue, N. M. *J. Phys. Chem. A* **2008**, *112*, 13535–13541.

Ozone Oxidation of B[*a*]P. B[*a*]P has been observed to form diones, hydroxy species, and the epoxide species B[*a*]P-4,5-oxide upon exposure to O_3 in laboratory studies and in atmospheric aerosol (refer to Figure 6 for the B[*a*]P labeling scheme).[4,66−68] B[*a*]P diones likely form via an O_3 oxidation mechanism related to pathway 1 for anthracene, with carbonyl formation at a given site initiating with O_3 addition to an adjacent C=C bond to form a primary ozonide. Hydroxy-B[*a*]P and B[*a*]P epoxides may also form via decomposition of the primary ozonide.

Table 6 lists the energetics of primary ozonide formation at different reaction sites on B[*a*]P, illustrated in Figure 7. As expected on the basis of our observations for anthracene and pyrene, formation of the primary ozonide at zigzag sites (see species b and c in Figure 7) requires some deformation from planar geometry, but addition of O_3 to edge sites does not (e.g., species a, Figure 7). Addition at the edge site *e* and at the zigzag site *g* is thermodynamically favorable, with $\Delta G_{rxn} = -26.5$ kcal mol^{-1} and −8.51 kcal mol^{-1}, respectively. Since the primary ozonide formed by addition at site *g* (species b in Figure 7) is only slightly distorted from the planar geometry of B[*a*]P, the energy penalty incurred for partial desorption is small. Thus, this pathway is thermodynamically favorable for each of the particle types studied here. O_3 addition to the zigzag site *h*, the armchair site at position *n*, or the internal bond (species c, d, and e in Figure 7) is not thermodynamically favorable, and the primary ozonides formed are nonplanar, further increasing ΔG. Therefore, we conclude that dione, hydroxy, and epoxide formation is most likely to occur at edge sites or the zigzag site at position *g*. This is consistent with observations of B[*a*]P-4,5-oxide and B[*a*]P-6,12-dione in atmospheric particles.[4,66]

Lactone formation has also been observed for B[*a*]P deposited on glass fiber filters.[68] Like open-ring compounds, lactone formation proceeds via the formation of a Criegee intermediate. On the basis of the observations of Letzel et al., and by analogy to pyrene, O_3 attack followed by Criegee intermediate formation will occur at the edge site *e*. On the basis of our calculations, Criegee intermediate formation at that position is thermody-

(66) Allen, J. O.; Dookeran, N. M.; Taghizadeh, K.; Lafleur, A. L.; Smith, K. A.; Sarofim, A. F. *Environ. Sci. Technol.* **1997**, *31*, 2064–2070.
(67) Pitts, J. N.; Vancauwenberghe, K. A.; Grosjean, D.; Schmid, J. P.; Fitz, D. R.; Belser, W. L.; Knudson, G. B.; Hynds, P. M. *Science* **1978**, *202*, 515–519.
(68) Letzel, T.; Rosenberg, E.; Wissiack, R.; Grasserbauer, M.; Niessner, R. *J. Chromatogr. A* **1999**, *855*, 501–514.
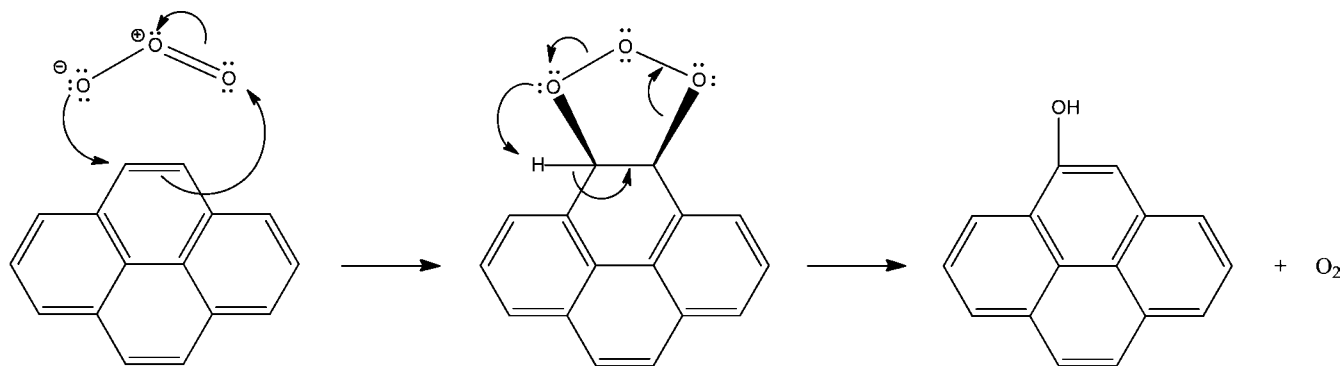
Figure 5. Proposed pyrene ozonolysis mechanism for the formation of hydroxypyrene.
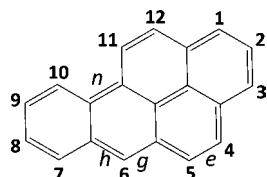
Figure 6. IUPAC labeling scheme for benzo[*a*]pyrene. For clarity, only edge sites discussed in the text are specified here.

Table 6. Energetics of Benzo[*a*]pyrene Primary Ozonides Shown in Figure 7

species	ΔG_{rxn} (kcal mol^{-1}) B3LYP/6-31G**	degree of desorption, ζ	$\Delta G_{rxn} + \zeta\Delta G_{des}$ (kcal mol^{-1})			
			fly ash	soot	NaCl	urban aerosol
a	−26.5	0		−26.5		
b	−8.51	1/20	−6.95	−7.06	−7.37	−7.40
c	+9.21	2/20	+12.3	+12.1	+11.5	+11.4
d	+22.3	11/20	+39.5	+38.4	+34.9	+34.6
e	+27.9	3/20	+32.6	+32.3	+31.3	+31.2

namically favorable, with $\Delta G_{rxn} = -26.6$ kcal mol^{-1} compared to the reactants (B[*a*]P and O$_3$). The Criegee intermediate is nonplanar ($\zeta = 0.8$), resulting in an energy penalty of 23.3 kcal mol^{-1} for B[*a*]P on soot (the substrate with the strongest B[*a*]P−surface interaction). The energy penalty is similar in magnitude to ΔG_{rxn}, but Criegee intermediate formation at this position is still predicted to be thermodynamically favorable when B[*a*]P is adsorbed on soot, fly ash, urban aerosol, or NaCl. That B[*a*]P lactone has not, to our knowledge, been observed in atmospheric aerosols suggests that its formation may be kinetically limited.

Insights for Graphene. Benzo[*a*]pyrene is a useful model compound for understanding graphene oxidation because it contains each of the nondefect oxidation site types present in graphene (edge, zigzag, armchair, internal). On the basis of this study, and B[*a*]P O$_3$ oxidation products reported in the literature, O$_3$ addition is expected to occur primarily at edge and zigzag sites for graphene. Functional groups expected to form during exposure of surface-deposited graphene to O$_3$ include carbonyl groups, edge epoxides, hydroxyl groups, and possibly lactones. The variety of possible functional groups suggests that O$_3$ oxidation is unlikely to be useful for targeted functionalization of graphene. Graphene is commonly assumed to be decorated on the edge with carboxylic acid groups.[69,70] This

has been observed to be true for graphene sheets prepared via oxidation of carbon nanotubes in solution.[71,72] If the graphene−substrate interaction is sufficiently strong, the formation of lactones, carboxylic acid groups, or other open-ring moieties after surface deposition may not be thermodynamically favorable.

On the basis of our findings, we predict that graphene should be relatively stable when subject to atmospheric aging by O$_3$. The O$_3$ oxidation reactions studied here would not lead to extensive carbon loss (lactone formation may result in loss of one carbon atom), and the sample will become passivated once the edge and zigzag sites are functionalized. However, Lee et al. found that that ozone chemisorption on the graphene basal plane resulting in epoxide formation would be weakly thermodynamically favorable ($\Delta G_{rxn} = -1.85$ kcal mol^{-1}) and observed graphite surface modification after exposure to very high gas-phase concentrations of O$_3$ (22 wt %) at 500 K.[73] This is in contrast to observations of B[*a*]P oxidation at atmospherically relevant conditions in the literature and our calculations, which indicate that the internal bond of B[*a*]P is stable. Further investigation into the oxidative aging of graphene by O$_3$ at environmentally relevant conditions is warranted. Oxidation by the hydroxyl radical (OH) should also be investigated for determining the environmental stability of graphene. OH has been observed to result in the volatilization via carbon loss of atmospheric aerosol organics, including pyrene.[74−76]

Conclusion

We have shown for the first time that steric effects on the PAH−substrate interaction may influence the mechanisms and products of PAH oxidation by O$_3$ on surfaces. We find that the formation of intermediates or products that do not conform to the planar geometry of the parent PAH molecule may be inhibited by attractive interactions with the underlying substrate. PAH−aerosol interactions may influence the atmospheric lifetimes of PAHs and the oxidation products formed. Our results also suggest that the oxidative aging of graphene by O$_3$ may result in a variety of functional groups at edge and zigzag sites.

(69) Fuente, E.; Menendez, J. A.; Diez, M. A.; Suarez, D.; Montes-Moran, M. A. *J. Phys. Chem. B* **2003**, *107*, 6350–6359.
(70) Al Aqtash, N.; Vasiliev, I. *J. Phys. Chem. C* **2009**, *113*, 12970–12975.
(71) Yuge, R.; Zhang, M. F.; Tomonari, M.; Yoshitake, T.; Iijima, S.; Yudasaka, M. *ACS Nano* **2008**, *2*, 1865–1870.
(72) Salzmann, C. G.; Nicolosi, V.; Green, M. L. H. *J. Mater. Chem.* **2010**, *20*, 314–319.
(73) Lee, G.; Lee, B.; Kim, J.; Cho, K. *J. Phys. Chem. C* **2009**, *113*, 14225–14229.
(74) Molina, M. J.; Ivanov, A. V.; Trakhtenberg, S.; Molina, L. T. *Geophys. Res. Lett.* **2004**, *31*, L22104 (DOI: 10.1029/2004GL020910).
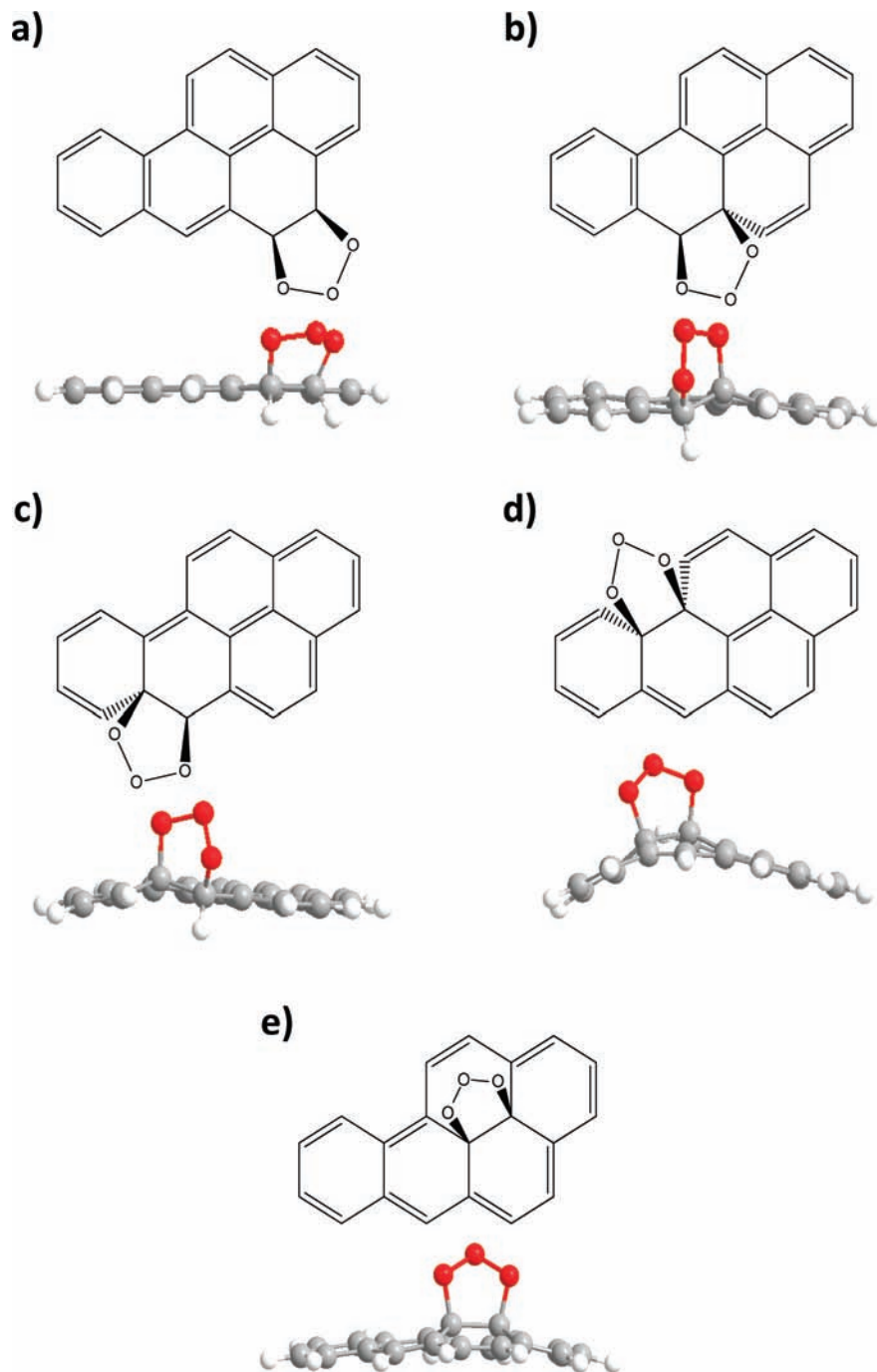(75) McNeill, V. F.; Yattavelli, R. L. N.; Thornton, J. A.; Stipe, C. B.; Landgrebe, O. *Atmos. Chem. Phys.* **2008**, *8*, 5465–5476.
(76) Vlasenko, A.; George, I. J.; Abbatt, J. P. D. *J. Phys. Chem. A* **2008**, *112*, 1552–1560.

Figure 7. Primary ozonides for benzo[*a*]pyrene.

Supporting Information Available: Comparison of calculated bond lengths and energies with experimental data, stoichiometry for formation of the anthracene oxidation products, and the optimized geometries and energies for all species. This material is available free of charge via the Internet at http://pubs.acs.org.

JA1014772